

SUPERCONDUCTING CAVITIES

W. Weingarten

CERN, Geneva, Switzerland

ABSTRACT

Most of the features of a superconducting cavity can be traced back to its low RF losses. The shunt impedance for acceleration is very high and so is the total efficiency of RF-to-beam power conversion. The cavity surface exposed to RF has to be absolutely clean and free of defects. Damping of the higher-order modes is essential for a cavity installed in an accelerator. The low bandwidth requires precise frequency tuning and sheet metal manufacturing demands precise field flatness tuning. The transfer of high RF power to the beam at low temperatures and the extraction of the beam induced higher-order mode power necessitates careful design of the cavity and of the cryostat.

1. INTRODUCTION

As this CERN Accelerator School is dedicated to "RF Engineering For Particle Accelerators", I will restrict this chapter to accelerating cavities and ideas linked with RF and not discuss materials or diagnostic techniques since these were covered in detail in a recent CERN Accelerator School [1]. Furthermore, I will restrict myself to a few individual topics, some of which were already published elsewhere [2]. My view is, of course, strongly biased towards techniques developed at CERN, which is why most of the examples come from there. I do not want to imply these are the best solutions, I have chosen them simply because I know them best.

2. THE RF-TO-BEAM POWER CONVERSION EFFICIENCY

Electrical power from the mains is transferred to the beam via the following chain: high-voltage power supply – klystron – waveguide – RF cavity – beam. For the time being, the largest power loss occurs between the RF cavity and the beam. In producing the accelerating voltage V in the cavity, RF currents are induced at its surface causing heating by the power loss P_c . A shunt impedance

$$R = V^2/(2 P_c) \quad (1)$$

is defined to account for these RF losses and should be as large as possible. RF accelerating cavities manufactured from high-conductivity copper have shunt impedances of typically $5 \text{ M}\Omega$ per cell at 352 MHz. With a beam current I_b and a power transferred to the beam $P_b = VI_b$, the conversion efficiency is defined as

$$\eta = P_b/(P_b + P_c) = 1/(1 + P_c/P_b) = 1/[1 + V/(2 RI_b)] . \quad (2)$$

For typical accelerating RF cavities made from copper with $R = 43 \text{ M}\Omega$, $I_b = 6 \text{ mA}$, $V = 3 \text{ MV}$ we get $\eta \approx 15\%$. As can be inferred from Eq. (2), normal conducting (n.c.) cavities made from Cu offer high conversion efficiencies for high beam currents and low accelerating voltages. It is the large "improvement factor" of the shunt impedance ($\sim 10^5$) compared to conventional Cu cavities which makes superconducting (s.c.) cavities so attractive.

However, the dissipated power $\dot{Q}_2 = P_c$ (Fig. 1) has to be removed at cryogenic temperatures, in common practice at the boiling temperature of liquid helium under normal pressure, $T_2 = 4.2$ K. Hence, the entropy current $S = \dot{Q}_2/T_2$, which, according to the second law of thermodynamics, in the ideal (reversible) case equals Q_1/T_1 at room temperature $T_1 = 300$ K. According to the first law of thermodynamics the power

$$\dot{W}_C = \dot{Q}_1 - \dot{Q}_2 = \dot{Q}_2 (\dot{Q}_1/\dot{Q}_2 - 1) = \dot{Q}_2 (T_1/T_2 - 1) \quad (3)$$

flows into the compressor. The Carnot efficiency η_C for a refrigerator is defined as

$$\eta_C = \dot{Q}_2 / \dot{W}_C = T_2 / (T_1 - T_2). \quad (4)$$

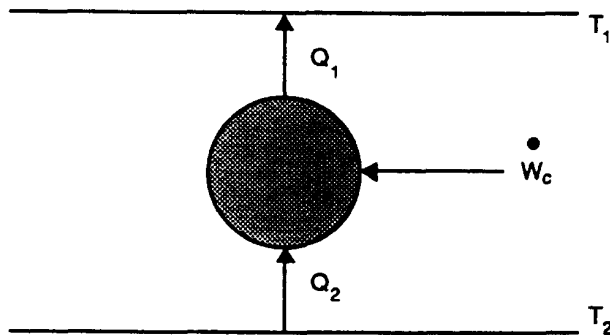


Fig. 1 Schematic power flow in a refrigerator

For $T_1 = 300$ K and $T_2 = 4.2$ K, $\eta_C = 1/70$. The “thermodynamic efficiency”

$$\eta_{td} = \dot{W}_C / \dot{W} \quad (5)$$

is the ratio of the power \dot{W}_C needed to operate the compressor in the ideal case to the “real” power \dot{W} . The total cryogenic efficiency is

$$\eta_{cr} = \dot{Q}_2 / \dot{W} = (\dot{Q}_2 / \dot{W}_C) (\dot{W}_C / \dot{W}) = \eta_C \eta_{td}. \quad (6)$$

With $\eta_{td} \approx 0.2$ for large units [3] the total cryogenic efficiency is $\eta_{cr} = 3 \cdot 10^{-3}$. Unavoidably, in an s.c. accelerator some power P_{cr} flows into the liquid He, even in the absence of RF (stand-by heat load of cryostat and He distribution system). The efficiency η of RF power to beam power conversion for an s.c. accelerator is then

$$\eta = [1 + (P_c + P_{cr})/(P_b \eta_{cr})]^{-1}. \quad (7)$$

As an example, for the s.c. cavity and cryostat for LEP with $P_c = 50$ W, $P_b = 50$ kW, $P_{cr} = 25$ W we get $\eta = 67\%$, which is by a factor of ~ 5 larger than for a conventional RF system.

3. THE ANOMALOUS SKIN EFFECT

As a starting point one can ask: why do we not build an accelerating cavity from high-purity copper, for instance, and cool it down to low temperatures to reduce its RF losses? Since for high-purity copper the increase in conductivity σ (residual resistivity ratio RRR) is 5000, one might expect that the RF losses decrease by $\sqrt{5000} \approx 70$. Unfortunately, the RF losses do not follow $1/\sqrt{\sigma}$ (normal skin effect), as one might expect, due to the anomalous skin effect (Fig. 2).

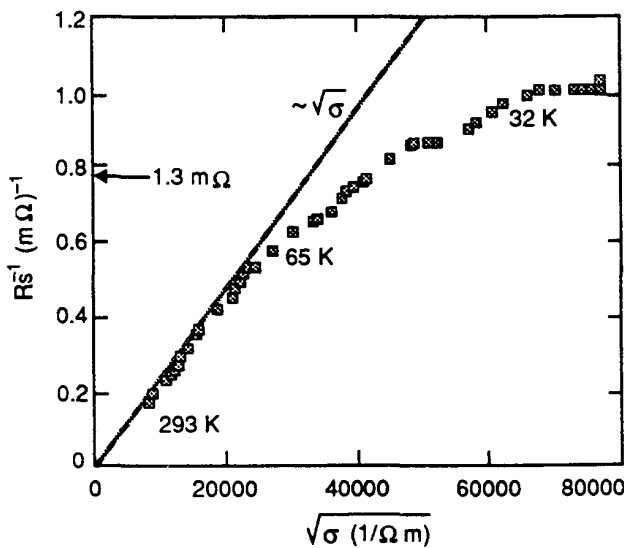


Fig. 2 Anomalous skin effect in a 500 MHz Cu cavity

The skin effect in a general sense is created by surface currents in the metal which short-circuit the electric field parallel to the surface. The domain of the anomalous skin effect is at low temperatures, where the mean-free path of the electrons l gets larger. Only electrons, whose free path l ranges within a surface layer where a non-vanishing electric field is present (the effective penetration depth δ_{eff}) contribute to the shielding current, the others are “invisible” to the electric field (Fig. 3). Hence, the effective density of electrons is reduced by the factor $\alpha(\delta_{\text{eff}}/l)$, with α a phenomenological factor near unity ($\approx 3/2$). The effective conductivity is, therefore, given by

$$\sigma_{\text{eff}} = \alpha(\delta_{\text{eff}}/l)\sigma.$$

Introducing this into the formula for the skin depth (Table 1), we obtain

$$\delta_{\text{eff}} = (2l/(\mu_0\omega\alpha\sigma))^{1/3}.$$

Similarly, the effective surface resistance R_{eff} for the anomalous skin effect is

$$R_{\text{eff}} = (\omega\mu_0/(2\sigma_{\text{eff}}))^{1/2} = (\omega\mu_0/2)^{2/3}(l/\sigma)^{1/3}\alpha^{-1/3},$$

which is, as $1/\sigma = \text{const.}$, independent of σ and exhibits the characteristic frequency dependence ($\sim \omega^{2/3}$) of the surface resistance in the anomalous limit. With typical values for a standard metal [4], $\sigma/(\Omega\text{m})^{-1} = 1.21 \cdot 10^{15} (\text{l/m})$, we obtain at 500 MHz, $R_{\text{eff}} = 1.3 \text{ m}\Omega$ (Fig. 2), which represents only a gain of a factor 4 compared to room temperature — independent of the conductivity at low temperature.

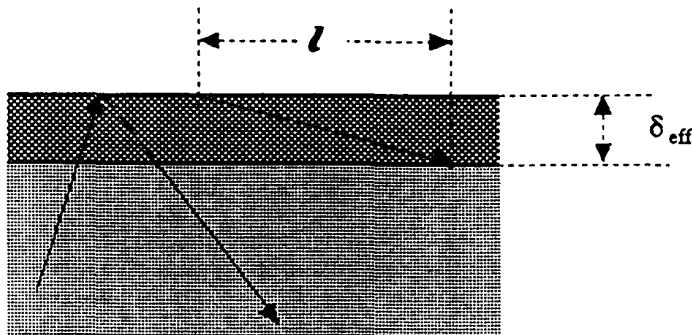


Fig. 3 Only electrons within the effective penetration depth contribute to shielding

Table 1
Comparison of superconductor (two-fluid model) with normal conductor

Superconducting metal	Normal conducting metal
$\operatorname{curl} \vec{H} = \vec{j} + \epsilon_0(d/dt)\vec{E}$ $\operatorname{curl} \vec{E} = -\mu_0(d/dt)\vec{H}$ $\operatorname{div} \vec{H} = 0$ $\operatorname{div} \vec{E} = 0$	
$(d/dt)\vec{j} = \vec{E}/(\mu_0\lambda_L^2) + \sigma_n(d/dt)\vec{E}$ $\operatorname{curl} \vec{H} = -\vec{H}/\lambda_L^2 - \sigma_n\mu_0(d/dt)\vec{H}$	$\vec{j} = \sigma_n\vec{E}$
$\Delta \vec{E} = -K^2\vec{E}$ $\Delta \vec{H} = -K^2\vec{H}$	
$K^2 = -\lambda_L^{-2}(1 - j\sigma_n\mu_0\omega\lambda_L^2 - \epsilon_0\mu_0\omega^2\lambda_L^2)$ $Z_{ss.c.} = (1/2)\omega^2\mu_0^2\lambda_L^3\sigma_n + j\omega\mu_0\lambda_L$ $\epsilon_0\mu_0\omega^2\lambda_L^2 \ll \sigma_n\mu_0\omega\lambda_L^2 \ll 1$	$K^2 = \epsilon_0\mu_0\omega^2(1 + j\sigma_n/(\omega\epsilon_0))$ $Z_{sn.c.} = (\omega\mu_0\delta/2)(1 + j) =$ $\sqrt{[\omega\mu_0/(2\sigma_n)](1 + j)}, \omega\epsilon_0/\sigma_n \ll 1$
Effective electron mass m Electron mean free path l Conductivity of the n.c. electrons $\sigma_n = ln_n e^2/(mv_F)$ London penetration depth $\lambda_L = \sqrt{[m/(n_s e^2 \mu_0)]}$	Surface impedance $Z_s = (E_z/H_y) _{x=0} = \mu_0\omega/K$ Skin depth $\delta = \sqrt{[2/(\mu_0\sigma_n\omega)]}$ Fermi velocity v_F Density of n.c. electrons n_n Density of s.c. electrons n_s

4. THE SURFACE IMPEDANCE OF SUPERCONDUCTORS

Another way to decrease the surface resistance is to make use of an s.c. surface. It is well known that the DC resistivity of a superconductor falls to zero below a critical temperature T_c . For RF, however, a non-zero surface resistance remains, which decreases with lower temperature. The two-fluid model of a superconductor is appropriate in understanding this. Suppose there are two fluids of electrons in the superconductor, the n.c. ones with density n_n and the s.c. ones with density n_s . Electric fields, if there are any, will drive currents through the two fluids, as they do through two impedances in parallel. The familiar Maxwell equations in a metal have to be completed by a combination of the London equations and Ohm's law.

The London equations are the constitutive equations for a superconductor. They give a mathematical description for the experimentally observed infinite DC conductivity and the Meissner–Ochsenfeld effect [5], which says that a (not too large) magnetic DC field is expelled from the material in the s.c. state.

The force which an electric field \vec{E} exerts on an s.c. electron $e\vec{E}$ will accelerate it according to Newton's law

$$m(d/dt)\vec{v} = e\vec{E}. \quad (8)$$

With the current density $\vec{j} = e n_s \vec{v}$, \vec{v} being the velocity vector of the s.c. electrons, we get the first London equation [6]

$$(d/dt) \vec{j} = (e^2 n_s / m) \vec{E} . \quad (9)$$

By applying the curl of Eq. (9) and taking into account one of Maxwell's equations,

$$(d/dt) \operatorname{curl} \vec{j} = (e^2 n_s / m) \operatorname{curl} \vec{E} = -(e^2 n_s / m) (d/dt) \vec{B} . \quad (10)$$

Hence, $\operatorname{curl} \vec{j} + (e^2 n_s / m) \vec{B}$ is independent of time and remains constant everywhere. The second London equation [6] states that this constant is zero

$$\operatorname{curl} \vec{j} + (e^2 n_s / m) \vec{B} = 0 . \quad (11)$$

With $\operatorname{curl} \vec{H} = \vec{j}$ for static fields, and $\mu_0 \vec{H} = \vec{B}$, we have a differential equation that describes the Meissner–Ochsenfeld effect

$$\operatorname{curl} \operatorname{curl} \vec{H} + \lambda_L^{-2} \vec{H} = 0 , \quad (12)$$

with $\lambda_L = \sqrt{[m/(e^2 n_s \mu_0)]}$. \vec{H} decays to zero in the superconductor within a characteristic length λ_L , the London penetration depth.

In Table 1 the equations for the two-fluid model are contrasted with those for a normal conductor. Skipping the detailed derivation, the surface resistance of a superconductor is

$$R_{ss.c.} = (1/2) \omega^2 \mu_0^2 \lambda_L^3 \sigma_n . \quad (13)$$

For $T < T_c/2$, n_n can be approximated by a Boltzmann factor $n_n \sim e^{-\Delta/(kT)}$, with $\Delta = 1.95 kT_c$ for Nb ($T_c = 9.25$ K), thus taking into account the pairing energy 2Δ for breaking a Cooper pair. Hence, the surface resistance is $R_{ss.c.} = A \omega^2 e^{-\Delta/(kT)}$, with A a function of the parameters of the normal conductor n_n , l , m and v_F . This result is roughly the one from the BCS theory [7]

$$R_{ss.c.}^{\text{BCS}} = (A'/T) \omega^2 e^{-\Delta/(kT)} . \quad (14)$$

Figures 4 and 5 show the temperature and frequency dependence of the surface resistance, respectively. It is evident that superconductors with a larger pairing energy 2Δ (higher T_c) should allow a smaller surface resistance at the same temperature, provided A' is about the same. This is the reason why the conventional and new high T_c superconductors such as Nb₃Sn and YBaCuO are being investigated for RF applications. The surface resistance of commercially available Nb is given by

$$R_{ss.c.}/n\Omega = 10^5 (f/\text{GHz})^2 \exp(-18/(T/\text{K}))/((T/\text{K})) .$$

For Nb₃Sn coated cavities ($T_c = 18.1$ K) we have

$$R_{ss.c.}/n\Omega = 10^5 (f/\text{GHz})^2 \exp(-40/(T/\text{K}))/((T/\text{K})) .$$

For comparison, the surface resistance for Cu at room temperature is $R_s/m\Omega = 7.8 (f/\text{GHz})^{1/2}$, 10⁵ times larger than for Nb at 4.2 K and 350 MHz. Consequently, the shunt impedance is larger by the same factor for s.c. cavities.

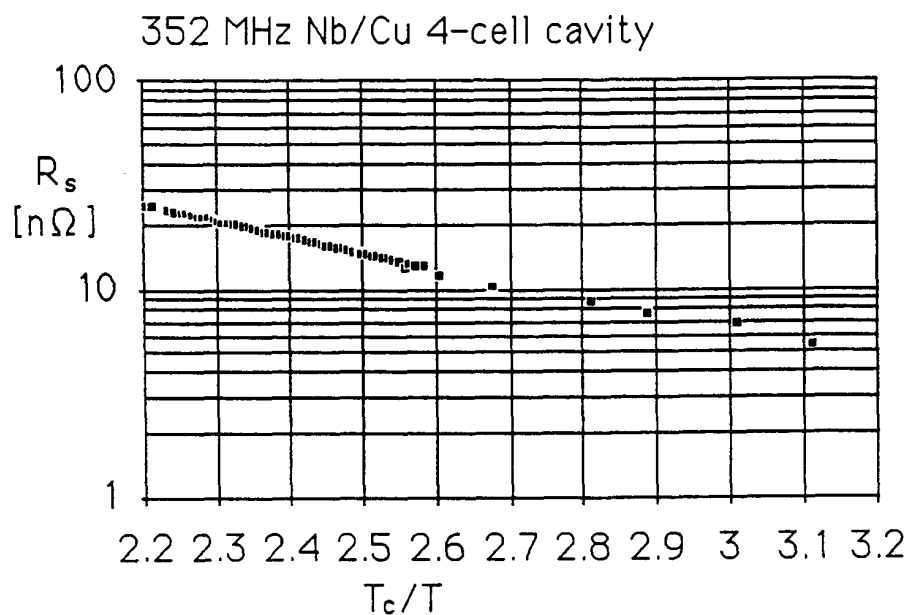


Fig. 4 RF surface resistance vs temperature

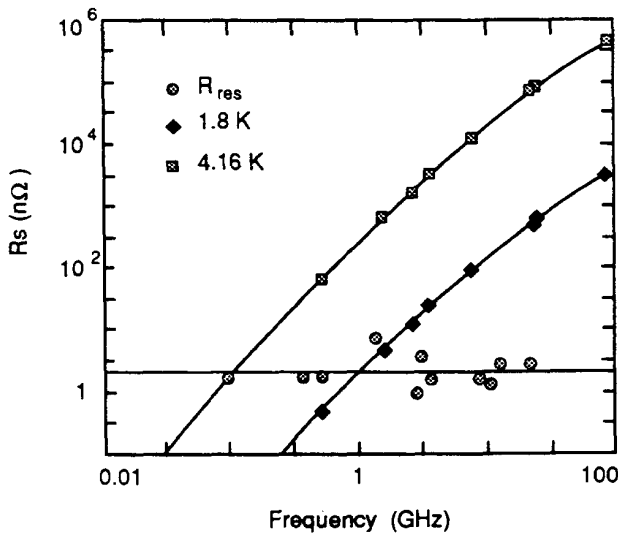


Fig. 5 RF surface resistance vs frequency

The two-fluid model, although not giving precise results, has the virtue of creating the correct frequency and temperature dependence and shows that the coefficient A' is related to the conductivity of the n.c. electrons.

It is instructive to check the validity of the approximations made to derive the s.c. surface impedance in Table 1, by inserting numbers for the standard metal. With

$$\sigma_n(300 \text{ K}) = 7.6 \cdot 10^6 (\Omega \text{m})^{-1},$$

a typical value for Nb,

$$\sigma_{n\text{eff}}(4.2 \text{ K})/(\Omega \text{m})^{-1} = 9.4 \cdot 10^8 / (f/\text{GHz})^{1/3},$$

$$n_n(300 \text{ K}) = 6 \cdot 10^{28} \text{ m}^{-3},$$

$$n_s(4.2 \text{ K}) \approx n_n(300 \text{ K}),$$

$$\epsilon_0 \mu_0 \omega^2 \lambda_L^2 = 2 \cdot 10^{-13} (\text{f/GHz})^2 \ll \sigma_{\text{neff}} \omega \mu_0 \lambda_L^2 \approx 3.5 \cdot 10^{-3} (\text{f/GHz})^{2/3} \ll 1.$$

Hence, for frequencies $f < 10 \text{ GHz}$ the approximations are justified. The wave vector \vec{K} is purely imaginary with $|K| = 1/\lambda_L$. The RF wave penetrates into the metal for a distance λ_L , which is independent of the frequency and equal to the DC penetration depth.

5. THE CRITICAL FIELD OF SUPERCONDUCTORS

In Table 2 various kinds of critical fields are defined. At first glance one might suppose that the maximum achievable RF surface magnetic field is B_c for type-I and B_{c1} for type-II superconductors, where the DC magnetic field starts penetrating the s.c. material. This is not the case in RF for reasons which are not fully understood. It is believed that the creation of n.c. islands in the s.c. metal needs some time, which is larger than one RF period. The limiting field in RF superconductivity is therefore larger than B_c and B_{c1} , respectively, and is called the critical superheating field B_{sh} .

Table 2
Critical fields in DC and RF superconductivity

B_c	Critical magnetic field of type-I superconductor
B_{c1}	Lower critical magnetic field of type-II superconductor
B_{c2}	Upper critical magnetic field of type-II superconductor
B_{cth}	Thermodynamic critical field
B_{sh}	Superheating critical field
B_{exp}	Experimentally obtained maximum field in RF
An index "0" following any of the above symbols refers to the temperature $T = 0 \text{ K}$, tacitly assuming $B(T) = B_0 [1 - (T/T_c)^2]$.	

B_{sh} values for the superconductors Sn, In, Pb, Nb, Nb_3Sn — typical materials studied in RF superconductivity — are given in Table 3, and are compared with the maximum surface fields B_{exp} obtained so far. It can be concluded that for Pb for example, B_{exp0} clearly exceeds B_{cth0} , and is very close to B_{sh0} . For Sn, B_{exp} is identical to B_{cth} for several temperatures, whereas for Nb $B_{exp0} < B_{c10}$.

Table 3
Critical field of superconductors studied for RF

Material	T_c [K]	B_{cth0} [mT]	B_{c10} [mT]	B_{c20} [mT]	B_{sh0} [mT]	B_{exp0} [mT]	Refs
Sn	3.7	30.9	—	—	68	30.6	[8]
In	3.4	29.3	—	—	104	28.4	[9]
Pb	7.2	80.4	—	—	105	112	[10]
Nb	9.2	200	185	420	240	160	[11,12]
Nb_3Sn	18.2	535	≈ 20	2400	400	106	[13]

Hence, as limiting field for RF in type-I superconductors, the experimental results for Sn suggest B_{cth} , whereas the experimental results for Pb exclude B_{cth} and suggest B_{sh} . For Nb, the critical fields B_{c1} , B_{cth} , B_{c2} and B_{sh} are still too high to be obtained experimentally so far. The result on Nb_3Sn indicates that B_{c1} can be surpassed in RF. A series of experiments on small samples of Sn-In and In-Bi alloys indicates that the limiting field in RF is indeed B_{sh} for

type-I and type-II superconductors [9]. If this is confirmed in the future, then very high magnetic surface fields can, in principle, be hoped for in s.c. accelerating cavities. With typically 4 mT surface magnetic field per 1 MV/m accelerating gradient, the ultimate limit for Nb is then 60 MV/m, and for Nb₃Sn 100 MV/m.

6. DISCREPANCIES BETWEEN THEORY AND EXPERIMENT — ANOMALOUS LOSSES

As far as we have seen up to now, there should be no reason not to obtain accelerating fields of 60 MV/m in s.c. Nb cavities. By sufficiently lowering the temperature of the liquid He bath, the RF losses should be negligibly small. At 350 MHz and 2 K, as an illustration, the s.c. LEP accelerating cavity should have a Q value of $8 \cdot 10^{11}$ and dissipate only 30 W at 60 MV/m accelerating gradient. Unfortunately, there are phenomena, in general not directly linked with RF superconductivity, which make this goal hard to achieve. The most important are the following:

- the residual surface resistance;
- surface defects of localized enhanced RF losses;
- electron emission.

6.1 The residual surface resistance

The residual surface resistance R_{S0} takes into account all physical effects which create a deviation of the experimentally obtained surface resistance R_S from the one described by theory R_{SBCS} ,

$$R_S = R_{SBCS} + R_{S0}. \quad (15)$$

Hence, R_{S0} comprises a variety of effects, some of a trivial nature, others of a more fundamental one. As the residual resistance is very small, its relevant physical parameters are difficult to control experimentally. This is one of the areas where research is presently being pursued. The challenge is to improve the technology of cavity manufacturing and to reduce fabrication flaws and surface contamination, so that the “trivial” causes for residual loss are reduced to a minimum. This is in itself not an easy task as, for example, 1 ppm contamination of iron concentrated into large enough lumps, would already create the same RF loss as Nb at 4.2 K and 350 MHz. This stresses how important it is to avoid any contamination of the superconductor during reduction, refinement, casting, furnace treatment, rolling, welding, polishing, rinsing and final assembly.

In parallel to the improvements in cavity manufacturing, new diagnostic tools, which allow one to distinguish between different loss mechanisms, have been developed. One example is the “temperature mapping” technique for the spatial resolution of RF losses and their absolute determination [1].

A well-established loss mechanism is trapped magnetic flux due to the presence of a residual static magnetic field which can originate in different ways during cool down. Because of the large demagnetization factor of the wall of the s.c. cavity, there is no expulsion of the magnetic field at the transition from the n.c. to the s.c. state due to the Meissner–Ochsenfeld effect, or the expulsion is very small. The magnetic field B on 1 m² of cavity surface splits up into N “fluxoids” of typical radius of a penetration depth λ with a local magnetic field B_{c2}

$$N = B / (\pi B_{c2} \lambda^2). \quad (16)$$

Each fluxoid has a n.c. core with the section $\pi \xi^2$, where ξ is the coherence length of the Cooper pairs. Hence, the additional surface resistance R_m due to trapped magnetic flux is

$$R_m = N \pi \xi^2 R_n = (\xi / \lambda)^2 (B / B_{c2}) R_n = \kappa^{-2} (B / B_{c2}) R_n, \quad (17)$$

where R_n is the surface resistance of the metal in the n.c. state. With the Ginzburg-Landau parameter $\kappa = \lambda/\xi \sim 1$ for Nb, in order to have $R_m < R_s \approx 10^{-5} R_n$, we have to arrange that $B/B_{c2} < 10^{-5}$. This implies that for Nb the ambient magnetic field has to be shielded to give $B < 10^{-5}B_{c2} = 10^{-5} \cdot 240$ mT = 2.4 μ T. From Eq. (17) we conclude that extreme type-II superconductors ($\kappa \gg 1$) should be insensitive to trapped magnetic flux.

Other causes which may contribute to the residual loss will only be enumerated: rough surfaces, "weak" s.c. spots, imperfectly-cooled islands of surface coatings, thermoelectrically-induced currents producing trapped magnetic flux, dielectric losses, and others. Radio-frequency losses may also depend on RF field amplitude other than quadratically, which would be manifested by a non-horizontal $Q(E_a)$ curve. The lowest residual surface resistances obtained so far at different frequencies are listed in Table 4 and shown in Fig. 5.

Table 4
Lowest experimentally obtained residual
surface resistance R_{s0} of Nb cavities

Frequency [GHz]	R_{s0} [n Ω]	References
0.09	1.8	[14]
0.35	< 2.0(a)	[15]
0.5	1.91	[16]
1.36	6.5	[17]
2.8	< 1.0	[18]
3.0	4.0	[19]
3.7	1.75	[20]
8.6	1.8	[21]
10.5	1.5	[22]
12.7	3.0	[23]
21.5	< 3.0	[24]

(a) Sputter deposited Nb.

6.2 Surface defects of localized enhanced losses

Whereas in X-band cavities of relatively small surface exposed to the RF field (some square centimetres), high surface magnetic fields have been obtained two decades ago [21], this is not the case in larger cavities for accelerator application at lower frequencies. It was suspected long ago, that small n.c. surface defects with much higher RF losses, relatively widely dispersed, were the origin. If so, by statistical arguments, the probability to obtain high surface fields was much larger in small single-cell cavities of higher frequency. Furthermore, the number of tests performed with small cavities at high frequency was much larger, which made a test result with a very high surface field more probable.

In some experiments at CERN, hot spots of enhanced RF loss causing breakdown were detected and localized by temperature mapping, inspected under a scanning electron microscope [25] and then removed. It turned out that, for accelerating fields less than ~ 8 MV/m (on commercial grade Nb in 1980), to every hot spot there could be attributed a surface defect which clearly had induced the thermal breakdown. These included welding "beads", welding holes, chemical residues and n.c. inclusions of a diameter of typically 100 μ m.

Why do these defects cause a breakdown?

Suppose a defect consisting of a half sphere (radius r) of n.c. metal exposed to the RF field is embedded in an s.c. metal of wall thickness d and thermal conductivity λ (Fig. 6), cooled by liquid He to the temperature T_B . The defect represents a heat source of the strength Q [W]. Under certain assumptions ($r \ll d$, no temperature drop across the metal-liquid interface)

the problem is equivalent to a circular symmetric one with a heat source of twice the strength \dot{Q} , for which the heat conduction equation

$$\Delta T = 2(\dot{Q}/\lambda)\delta(r) \quad (18)$$

is solved by

$$T = \dot{Q}/(2\pi\lambda r) + T_B. \quad (19)$$

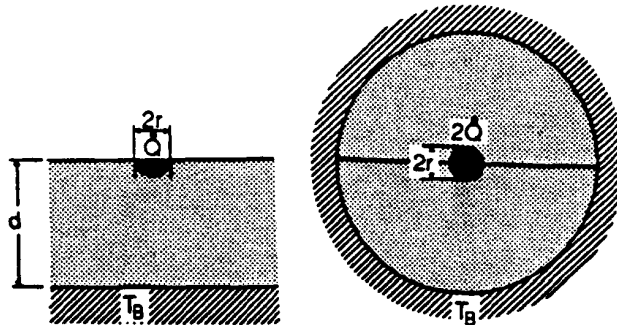


Fig. 6 Modelling the thermal breakdown (quench) caused by an n.c. defect producing heat at a rate \dot{Q}

The heat source strength is approximately

$$\dot{Q} = (1/2)R_n H^2\pi r^2, \quad (20)$$

where R_n is the surface resistance of the n.c. metal and H the local magnetic surface field. Hence,

$$T = (1/4)R_n H^2 r / \lambda + T_B. \quad (21)$$

Breakdown will occur when the temperature at the n.c. – s.c. interface approaches T_c . This gives a condition for the maximum RF field H_{max}

$$H_{max} = \sqrt{(4(T_c - T_B)\lambda/(R_n r))}. \quad (22)$$

With typical values $\lambda = 10 \text{ W/(mK)}$, $T_B = 1.8 \text{ K}$, $R_n = 40 \text{ m}\Omega$, $r = 10^{-4} \text{ m}$ we obtain $H_{max} = 20 \text{ mT}$, which corresponds to 5 MV/m accelerating gradient, in good agreement with the experimental results obtained a decade ago.

It was clear that, to increase the maximum surface field H_{max} , every effort should be undertaken to reduce the number and size of the surface defects and, on the other hand, make available s.c. metal of increased thermal conductivity (“thermal stabilization” of defects). This aim was accomplished by repeated furnace treatments and solid state gettering, which reduces the interstitial impurity content of all impurities present in Nb (O, N, H and C) contributing most significantly to the thermal conductivity [26].

Another way was to coat high thermal conductivity material such as OFHC Cu with a thin s.c. film of Nb or Pb of $\sim 1 \mu\text{m}$ thickness, thick enough by far to carry the supercurrent. As an example, LEP-type cavities sputter-coated with Nb [15] exhibit maximum accelerating fields and Q values comparable with, or even better than, Nb sheet metal (Fig. 7). These cavities have never been limited by a thermal breakdown. In addition, thanks to the structure of the sputter-coated layer they show nearly no extra RF loss due to trapped magnetic flux up to at least more than twice the earth's magnetic field, significantly alleviating the task of obtaining a low-residual surface resistance.

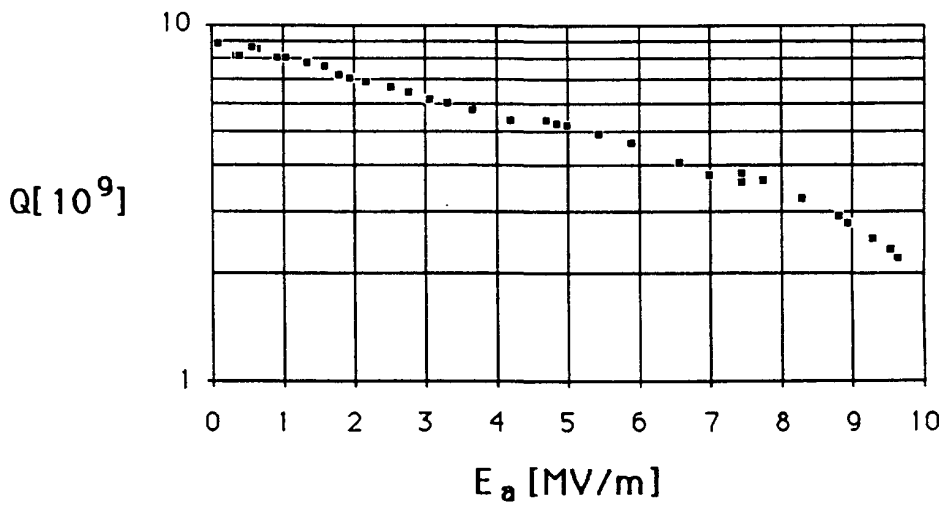


Fig. 7 Q vs accelerating field at 4.2 K of a LEP-type Nb sputter-coated Cu cavity at 350 MHz

6.3 Field emission electron loading

Since achieving the thermal stabilization of defects, thermal breakdown of s.c. cavities has become less frequent and the maximum fields obtained could be significantly increased. Other breakdown phenomena typical of higher electric fields such as electron emission, then gain importance. Electrons are emitted at the surface, accelerated in the electromagnetic field of the cavity and, when hitting the wall, give off their kinetic energy as heat and as bremsstrahlung. The result is a drastic decrease of the Q value known as “electron loading”.

Two mechanisms of electron emission in s.c. cavities could be confirmed experimentally: one by multipacting electrons, the other by field-emitted electrons.

Electron multipacting is a resonance phenomenon and is linked to the electric surface field, the secondary electron emission coefficient δ of the surface, the geometry of the cavity and the frequency. Properly cleaned Nb cavities (low δ) of rounded shape have been shown to be virtually free from multipacting [27].

Field emission of electrons from metallic surfaces is determined by the work function and, according to the Fowler–Nordheim law, should occur only at very large electric fields E (\sim GV/m). Unfortunately, DC field emission experiments showed that small ($< 1 \mu\text{m}$) non-metallic sites on Nb surfaces emit electrons at fields a factor β lower (“field enhancement” factor), and that β is of the order of some hundreds. There is no reason to believe that field emission in s.c. RF cavities is of a different nature though the origin is not yet understood. The field emission current can be parametrized by the Fowler–Nordheim law

$$j = (e^3/(16\pi^2\hbar))(E^2/\Phi)\exp[-(4/3)\sqrt{(2m)/(e\hbar)}\Phi^{3/2}/E]. \quad (23)$$

It is common practice to use as work function $\Phi = 4.3 \text{ eV}$ for Nb and $E = \beta E_s$, E_s being the macroscopic surface field. For j in 10^{12} A/m^2 and E in 10^{10} V/m ,

$$j = (6 E)^2 \exp(-6/E). \quad (24)$$

This equation makes it evident that j increases very rapidly with E for $E = \beta E_s > 10^{10} \text{ V/m}$. With a typical $\beta = 250$, the macroscopic surface field is $E_s > 40 \text{ MV/m}$, which corresponds to an acceleration field of $E_a > 20 \text{ MV/m}$. This is in the range of the maximum fields ever obtained in accelerating cavities.

Statistical arguments confirm the idea that sites emitting electrons at a lower field are less frequent than those emitting at a higher field. This argument gives a qualitative understanding of why it is more difficult to obtain higher fields in larger cavities at lower frequency [28]. Only the strict observation of “clean working” rules allows the emission process to be mastered at even higher surface fields. By “clean work” we mean a careful final processing of the cavity surface by rinsing with ultra-pure liquids such as water of the quality used in semiconductor manufacturing (Table 5) [29] and clean assembly under laminar dust-free airflow (class 100 or better).

Table 5
Water quality for semiconductor chip manufacturing

Item	Integration Units	Integration scale	64 kbits	256 kbits	1 Mbits	4 Mbits
Resistivity Particulates	[M Ω cm]		15 ... 16	17 ... 18	17.5 ... 18	18 ...
	[μm]		0.2	0.2	0.1	0.1
Bacteria	[Counts/ml]		50 ... 150	30 ... 50	10 ... 20	5 ... 10
	[Counts/100 ml]		50 ... 100	5 ... 20	1 ... 5	1
Total organic carbon	[ppb]		50 ... 200	50 ... 100	30 ... 50	20 ... 30
Silicon dioxide	[ppb]		20 ... 30	10	5	5
Oxygen	[ppb]		100	100	50...100	50

7. THE RESPONSE OF A SUPERCONDUCTING CAVITY TO RF

7.1 Basic parameters

In order to model the response of an s.c. cavity to RF, its fundamental parameters have to be defined. One possible set of these are the accelerating voltage V , the resonance frequency ω_0 , the stored energy U , the power P_c dissipated in the cavity itself, and the power radiated off the cavity P_{rad} at a given V . Having defined these, other characteristic parameters may be deduced, the most important being given in Table 6.

Table 6
Characteristic cavity parameters

Accelerating voltage	V
Resonant frequency	ω_0
Stored energy	U
Dissipated power	P_c
Radiated power	P_{rad}
Shunt impedance	$R = V^2/(2P_c)$
(Unloaded) Q value	$Q_0 = \omega_0 U / P_c$
External Q value	$Q_{\text{ext}} = \omega_0 U / P_{\text{rad}}$
(R/Q) value ^(a)	$R/Q = V^2/(2 \omega_0 U)$
(a) This is the definition used in RF circuit theory. Sometimes, in particular for linear accelerators, one finds the definition $R/Q = V^2/(\omega_0 U)$.	

The fundamental parameters V , ω_0 , U , P_c and P_{rad} have their exact equivalent in a lumped, parallel, resonant-circuit model shown in Fig. 8(a), and are listed in Table 7. R/Q is defined as in circuit theory. By refining this model further, the coupling to the outside world has

to be taken into consideration by, for instance, a loss-less transformer with turns ratio 1:n for the input coupler, as in Fig. 8(b).

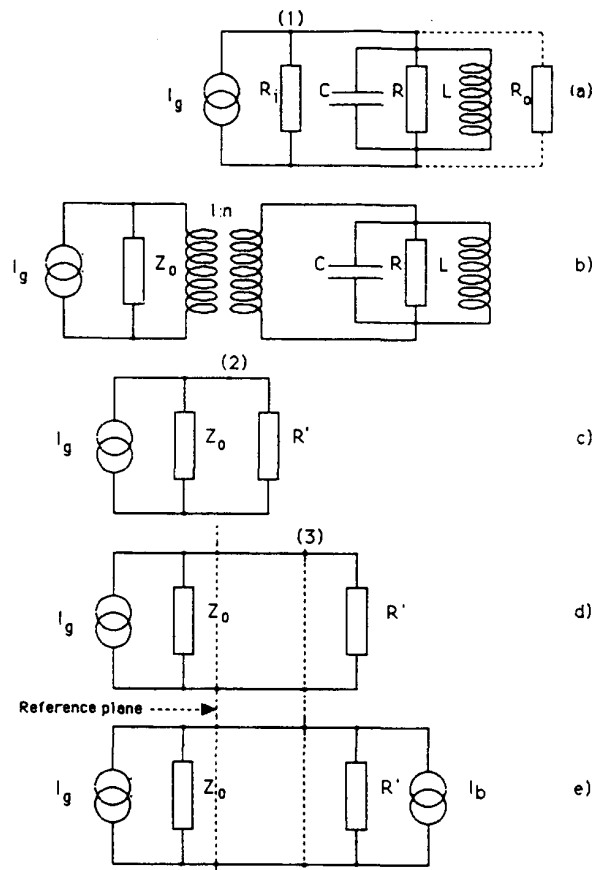


Fig. 8 Lumped element equivalent circuit model of an accelerating cavity resonator

Table 7
Equivalence of cavity and lumped-element circuit parameters

Cavity	Lumped-element circuit
Accelerating voltage V	Peak voltage V
Resonant frequency ω_0	$\omega_0 = 1/\sqrt{LC}$
Stored energy U	$U = (1/2) C V^2$
Dissipated power P_c	$P_c = (1/2) V^2/R$
Radiated power P_{rad}	$P_{rad} = (1/2) V^2/R_i$
Shunt impedance $R = V^2/(2P_c)$	R
(Unloaded) Q value $Q_0 = \omega_0 U / P_c$	$Q_0 = \omega_0 R C$
External Q value $Q_{ext} = \omega_0 U / P_{rad}$	$Q_{ext} = \omega_0 R_i C = R_i / (R/Q)$
(R/Q) value $R/Q = V^2/(2\omega_0 U)$	$R/Q = \sqrt{L/C} = 1/(\omega_0 C)$
Coupling factor $\beta = Q_0 / Q_{ext}$	$\beta = R/R_i$
Loaded Q value $Q_L = Q_0 / (1 + \beta)$	$Q_L = \omega_0 / (1 + \beta)$
Turns ratio $n = \sqrt{[(R/Q)Q_{ext}/Z_0]}$	$n = \sqrt{[R_i/Z_0]}$
Wave impedance $Z_0 = 50 \Omega$	

7.2 The circuit equation

The derivation of the circuit equation is straightforward by applying Kirchhoff's current law at location 1 of Fig. 8(a)

$$V/R_i + (1/L) \int V(t) + C(d/dt)V + V/R = I_{g0} \cos(\omega t). \quad (25)$$

After differentiating and with the help of Table 7 the lumped circuit parameters can be transformed into cavity parameters

$$(d^2/dt^2)V + (\omega_0/Q_L)(d/dt)V + \omega_0^2V = -I_{g0}(R/Q)\omega\omega_0 \sin(\omega t). \quad (26)$$

To solve this inhomogeneous differential equation one has to find first the general solution of the homogeneous equation (which describes the free oscillation of the circuit). It can be solved by standard methods

$$V(t) = \exp[-\omega_0 t/(2Q_L)] (c_1 \exp\{j\sqrt[1 - 1/(2Q_L)^2]\omega_0 t\} + c_2 \exp\{-j\sqrt[1 - 1/(2Q_L)^2]\omega_0 t\}). \quad (27)$$

To find the general solution of the inhomogeneous differential equation one has to add a particular integral PI of the inhomogeneous differential equation to the general solution of the homogeneous equation. One can find it by different well known methods: Ansatz, integrating factor, Laplace transform or series solution methods, variation of constants, or simply by guessing

$$PI = \left\{ I_{g0}(R/Q) / [(\omega_0/\omega - \omega/\omega_0)^2 + (1/Q_L)^2] \right\} [(1/Q_L) \cos(\omega t) - (\omega_0/\omega - \omega/\omega_0) \sin(\omega t)]. \quad (28)$$

Without loss of generality we can simplify as follows. First, we have a feedback circuitry available which locks the generator frequency ω to the resonant frequency of the cavity ω_0 : $\omega = \omega_0$. Secondly, we use the boundary conditions

$$\begin{aligned} V(t)|_{t=0} &= 0, \\ V(t)|_{t \rightarrow \infty} &= V_0 = I_{g0}(R/Q) Q_L \end{aligned}$$

and

$$1 - 1/(2Q_L)^2 \approx 1,$$

such that

$$V(t) = V_0 \cos(\omega_0 t) \{ 1 - \exp[-\omega_0 t/(2Q_L)] \}. \quad (29)$$

7.3 Observing the cavity response

For obvious reasons the observer will conduct his experiments outside the cavity probing the RF signals between generator and coupling network. So, let us imagine the observer will be located at position 2 of Fig. 8(c). V and R will be mapped by the ideal transformer (turns ratio n) into V'_0 and R' at position 2: $V'_0 = V_0/n$, $R' = R/n^2$. Suppose he looks at the incident and reflected waves, the voltage amplitudes of which are V'_+ and V'_- , and the current amplitudes I'_+ and I'_- . Let us assume that V'_0 , R' and $Z_0 = 50 \Omega$ (or its ratio $\beta = R'/Z_0$, respectively) are given and we wish to calculate the forward and reflected wave voltage amplitudes. It is well known from transmission line theory, that

$$V' = V'_+ + V'_-, \quad (30)$$

and

$$I' = I'_+ - L' . \quad (31)$$

We can define the reflection factor

$$\rho = V'_-/V'_+ , \quad (32)$$

from which we get

$$\rho = (R' - Z_0)/(R' + Z_0) . \quad (33)$$

Whereas the reflection factor depends on position, we are often interested in its absolute value, which does not (assuming loss-less cables),

$$\begin{aligned} |\rho| &= (\beta - 1)/(\beta + 1), \beta \geq 1 ; \\ &= (1 - \beta)/(1 + \beta), \beta \leq 1 . \end{aligned} \quad (34)$$

We would like to express the coupling factor β by $|\rho|$

$$\begin{aligned} \beta &= (1 - |\rho|)/(1 + |\rho|), \beta \leq 1 ; \\ &= (1 + |\rho|)/(1 - |\rho|), \beta \geq 1 . \end{aligned} \quad (35)$$

If we wish to establish a steady state voltage V'_0 in the cavity we use Eqs (30), (31) and (32) and find that the incident wave amplitude V'_+ is

$$V'_+ = (\beta + 1)/(2\beta) V'_0 . \quad (36)$$

The reflected wave amplitude $V'_-(t)$ is finally given by

$$\begin{aligned} V'_-(t) &= V'(t) - V'_+ = \\ &= V'_0 \left(\cos(\omega_0 t) \{ 1 - \exp[-\omega_0 t/(2Q_L)] \} - (\beta + 1)/(2\beta) \right) . \end{aligned} \quad (37)$$

The steady state voltage in the cavity V_0 is

$$V_0 = n V'_0 = V'_+ [2\beta/(\beta + 1)] \sqrt{[(R/Q)Q_{ext}/Z_0]} . \quad (38)$$

With the incident power

$$P_+ = V'_+^2/(2Z_0) \quad (39)$$

we end up with (mind the definition $R/Q = V^2/(2\omega_0 U)$!)

$$V_0^2 = [8\beta^2/(1 + \beta)^2](R/Q) Q_{ext} P_+ = [8\beta/(1 + \beta)^2](R/Q) Q_0 P_+ . \quad (40)$$

In Fig. 9 the cavity voltage $V'(t)$, the incident voltage $V'_+(t)$, and the reflected voltage $V'-(t)$ are shown for three different coupling factors $\beta = 1/3, 1$ and 7 .

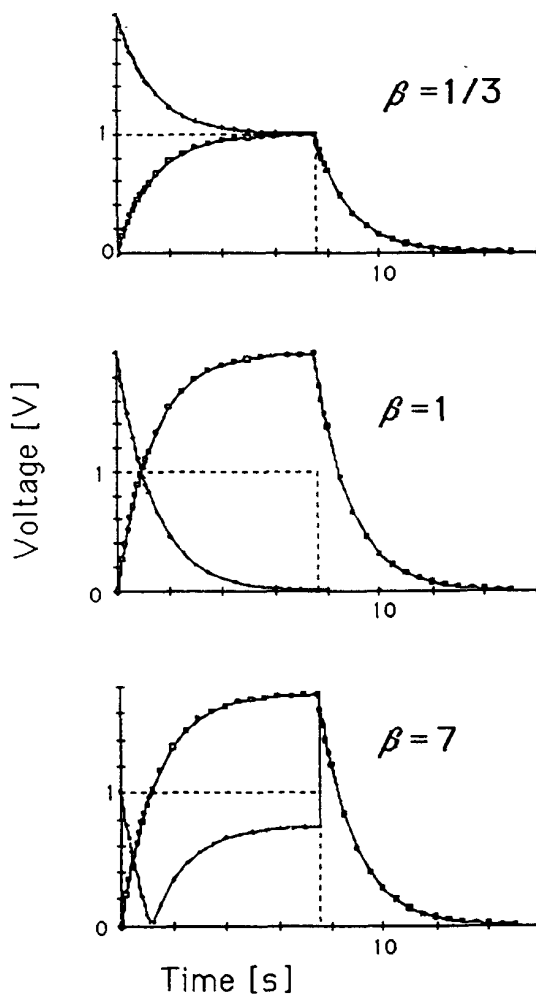


Fig. 9 The reflected and transmitted RF signals of a superconducting cavity with the coupling factor β as parameter ($Q_L = 1 \cdot 10^9$, $R/Q = 232 \Omega$, $f = 350$ MHz). The incident power pulse is indicated by the broken line.

If the cavity voltage is probed by a pick-up antenna and if the power P_{radout} leaving the cavity by the pick up probe is about of the same order of magnitude as the dissipated power P_c in the cavity, the equations given above need a slight modification. In the lumped-element equivalent circuit diagram of Fig. 8(a) the shunt resistance R has the resistance R_0 in parallel. This means that in the equations given above, the replacement $R \rightarrow (R^{-1} + R_0^{-1})^{-1}$, equivalent to $Q_0 \rightarrow (Q_0^{-1} + Q_{\text{extout}}^{-1})^{-1}$, has to be effectuated. Therefore, in practice P_{radout} is measured, and the dissipated power in the cavity P_c is replaced by $P_c \rightarrow P_c - P_{\text{radout}}$. And similarly, $Q_0 \rightarrow (Q_0^{-1} - Q_{\text{extout}}^{-1})^{-1}$, with $Q_{\text{extout}} = \omega_0 U/P_{\text{radout}} = V^2_0/(2(R/Q))/P_{\text{radout}}$.

Taking the quintessence of the formulae, the loaded Q value is determined from the $1/e$ decay time τ of the stored energy in the cavity (c.f. Eq. (29)) $U(t) = U_0 [1 - \exp(-\omega_0 t/Q_L)]$

$$Q_L = \omega_0 \tau. \quad (41)$$

From the absolute value of the reflection factor $|\rho|$ and Eq. (35) we get the coupling factor β and hence the unloaded Q value (c.f. Table 7)

$$Q_0 = (1 + \beta)Q_L, \quad (42)$$

and finally with the help of Eq. (40) the accelerating voltage V_0 . The average surface resistance is

$$R_s = G/Q_0 ,$$

with the so-called geometry factor G [1].

7.4 Diagnosing anomalous losses by observing the cavity response

Whenever there is a difference between the observed signals $V'_-(t)$ (and $V(t)$) and the ones shown in Fig. 9, the RF losses in the cavity no longer vary quadratically with the field. Therefore, $V'_-(t)$ (and $V(t)$) contain useful information on anomalous losses in the cavity. Although sometimes an unambiguous diagnosis on the cavity necessitates the observation of other complementary phenomena (temperature and X-ray maps, electron current, etc.) we can nevertheless often draw a conclusion on the status of a cavity from $V'_-(t)$ (and $V(t)$) alone. In other terms, $V'_-(t)$ contains the complete information on the unloaded Q value vs the accelerating voltage, Q_0 (V_0), implicitly.

8. COUPLING TO SUPERCONDUCTING CAVITIES

8.1 Coupling RF power into the cavity

Most of the RF input couplers used are of the coaxial line antenna type. Therefore, the coupling between the waveguide and cavity fields is produced by a time varying electric field. Paradoxically, it is a current (displacement current), which is injected by the coupler into the cavity. In the lumped-circuit diagram of Fig. 8 however, the coupling is via the magnetic field in a loss-less transformer. This model has the advantage of being instructive and simple. However, we have a price to pay for the convenient analogy of the cavity accelerating voltage and the lumped-circuit peak voltage in a parallel-circuit resonator. We do not want to give up this analogy, yet we have to take into account that this lumped-circuit model may be misleading in the vicinity of the coupling network.

We are able to save the analogy, nevertheless. We know from waveguide theory that by a shift on the line of a quarter wavelength we go from maximum magnetic field to maximum electric field and vice versa. That is why we introduce a reference plane in the transmission line between the generator and the cavity a quarter wavelength ahead of the coupler tip. There we know we have an analogy between the fields in the lumped circuit model and the coupling network (Fig. 8(d)). This gives us a means of knowing the distribution of fields along the coaxial line which is sometimes important in diagnosing parasitic RF losses. At location 3 of Fig. 8(d), for the cavity in the s.c. state and in full reflection (no beam, $R' \gg Z_0$), the reflection coefficient is $\rho = (R' - Z_0)/(R' + Z_0) = 1$. At the reference plane, however, a quarter wavelength ahead, or equivalently at the coaxial coupler tip, we have $\rho = -1$, which signifies a short circuit. There is a low impedance. The RF current (the magnetic field) is high, the RF voltage (the electric field) is zero. For the cavity in the n.c. state we mention, for the sake of completeness, that in general $Z_0 \gg R'$, $\rho = -1$ at location 3 and $\rho = 1$ at the reference plane, such that all these arguments are inverted.

By a well-controlled detuning of the cavity one can even shift the standing wave pattern along the coaxial line. This feature we used once at CERN in localizing the source of excess heating in the coaxial coupler. We found that the heating was maximum when the current maximum coincided with a joint in the line. We have to use a specially-designed gasket made from Cu there, in order to have tolerable RF losses.

The application determines the coupling layout. A useful number which depends only on the coupling geometry is the ratio of the stored energy and the radiated energy off the coupling hole within one cycle, the external Q value. It goes without saying that we always assume, if not otherwise mentioned, that this energy is completely absorbed by an external load (usually 50Ω), and nothing is reflected back into the cavity.

For most applications we wish to have “critical coupling” to the cavity: $\beta = 1$, which implies $Q_{\text{ext}} = Q_0$. (This condition minimizes the wasted reflected power). For laboratory testing, it minimizes the error made in determining the dissipated power in the cavity and so the unloaded Q value. We have therefore a weak coupling or a high $Q_{\text{ext}} = Q_0 = 10^9$ to 10^{10} . In an accelerator, most of the input power is transferred to the beam. In the lumped circuit model of Fig. 8(e) the (DC) beam current I_b (with peak RF component $2 I_b$) can be represented as a current source with current across a gap with the accelerating voltage V_a . Hence, on condition that voltage and current are in phase, it takes away the power P_b ,

$$P_b = (1/2) V_a^2 / R_b = (1/2) V_a (2 I_b) = V_a I_b , \quad (43)$$

by which an impedance R_b can be defined by

$$R_b = V_a / (2 I_b) . \quad (44)$$

In analogy to the previous discussion we had on the RF power leaving the probe antenna, we now have to make the replacement $R \rightarrow (R^{-1} + R_b^{-1})^{-1}$. We have critical coupling for $(R^{-1} + R_b^{-1}) = R_i^{-1} = [(R/Q)Q_{\text{ext}}]^{-1}$ or, as $R \gg R_b$,

$$Q_{\text{ext}} \approx (V_a / I_b) / (2 \cdot R/Q) . \quad (45)$$

For the LEP s.c. cavity with $V_0 = 8.5$ MV (taking without loss of generality the synchronous phase angle $\phi = 0$, such that $V_a = V_0 \cos \phi = V_0$), $I_b = 6$ mA and $(R/Q) = 232 \Omega$ we get $Q_{\text{ext}} = 3 \cdot 10^6$.

For a well-defined coupling geometry, i.e. a fixed Q_{ext} and a fixed forward power P_+ , we can ask how the cavity voltage depends on the beam current? From Eq. (40), and by taking into account the replacement $\beta = R/R_i \rightarrow (R^{-1} + R_b^{-1})^{-1}/R_i = 1/[Q_{\text{ext}}(Q_0^{-1} + (R/Q)2 I_b/V_0)]$, we have

$$[V_0 + Q_{\text{ext}}(V_0/Q_0 + 2(R/Q)I_b)]^2 = 8(R/Q)Q_{\text{ext}}P_+ . \quad (46)$$

As, in general, $(R/Q)I_b \gg V_0/Q_0$, we can simplify Eq. (46) to

$$[V_0 + Q_{\text{ext}} 2(R/Q)I_b]^2 = 8(R/Q)Q_{\text{ext}} P_+ , \quad (47)$$

a graph of which is shown in Fig. 10. Equation (47) tells us the importance of an RF input power coupler, by which Q_{ext} can be changed according to the beam current [30], in order to keep the accelerating voltage unchanged. A variable input power coupler is under development at CERN [31].

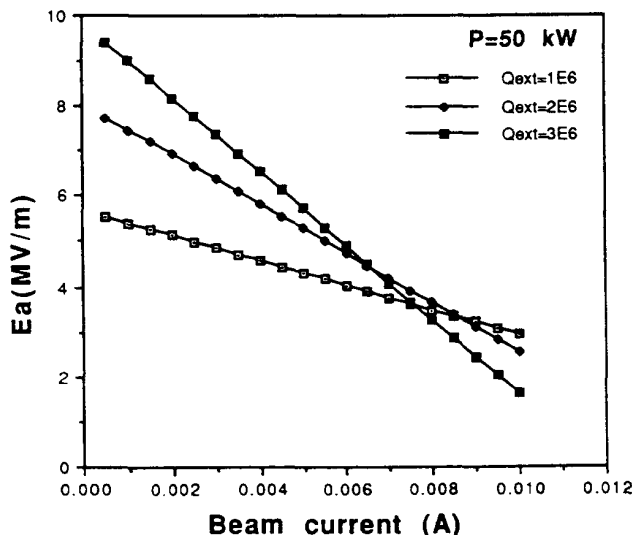


Fig. 10 Accelerating field vs beam current with Q_{ext} as parameter ($P_+ = 50$ kW, $R/Q = 232 \Omega$)

From Eq. (47) we see that for a test without beam

$$V_0^2 = 8 (R/Q) Q_{ext} P_+ . \quad (48)$$

Figure 11 shows the RF power coupler used at CERN [32]. It was tested at liquid He temperatures up to an input power of 50 kW on a 50Ω load.

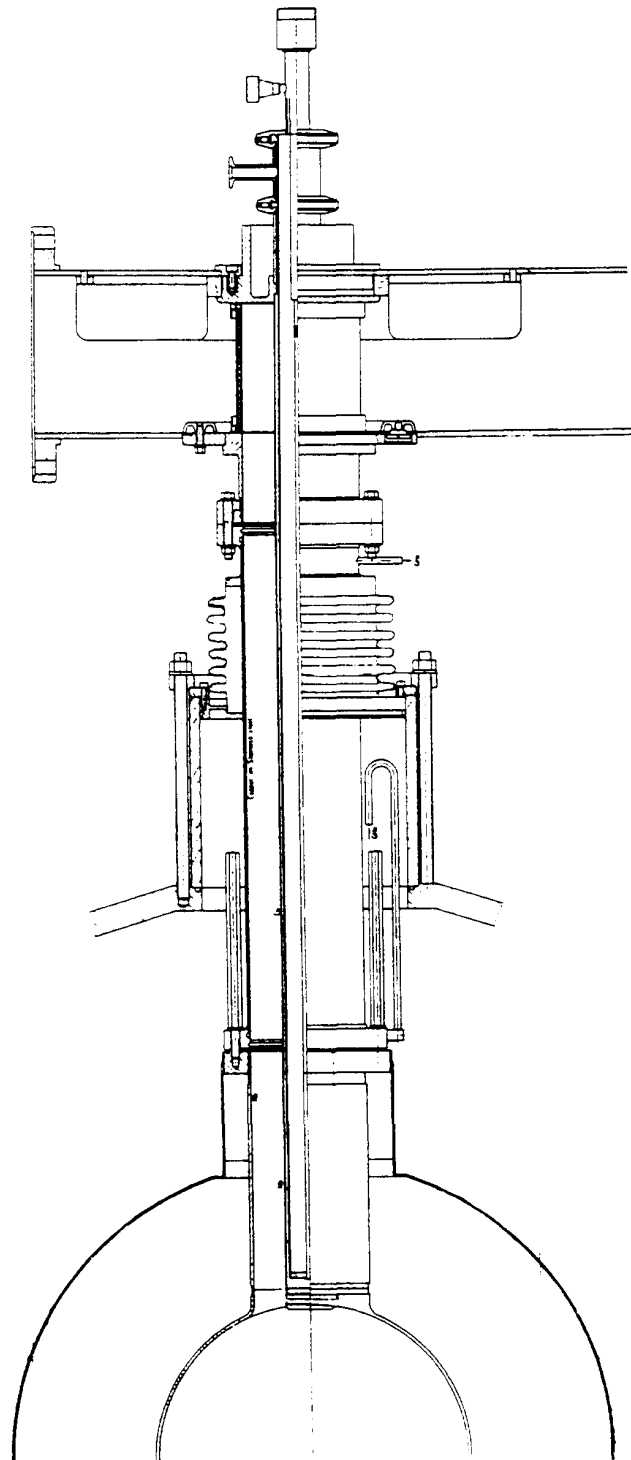


Fig. 11 Radio-frequency power coupler for LEP s.c. cavities

There are applications, for instance in LEP, where the RF power is generated in a 1 MW klystron and distributed in four stages to have ~ 50 kW available at a string of 16 s.c. cavities. This solution requires a circulator. On the other hand, for the SPS acting as an electron positron injector into LEP, the RF power is generated by one tetrode per cavity and does not require a circulator. It is worthwhile describing this latter solution in more detail [33]. The SPS is an accelerator where, in an interleaved cycle of 14.4 s, e^- and e^+ beams are accelerated for injection into LEP, and a proton beam is accelerated for fixed-target physics. The s.c. cavities already installed complement the existing RF system of n.c. cavities. They are operated at high voltage and relatively low current during the $e^- e^+$ acceleration, and at zero voltage and at relatively high current in the remaining cycle of p acceleration. These requirements for the RF amplifier are shown in Table 8. A tetrode producing 50 kW in a 50Ω load is perfectly able to cope with the two modes of operation.

Table 8
Modes of operation of the s.c. cavity in the SPS

Mode	Tetrode	Cavity
Conditioning of the cavity	10^4 V ~ 0 A	10^7 V ~ 0 A
e^\pm acceleration	10^4 V 1 A	10^7 V 10^{-3} A
p compensation	0 V 10 A	0 V 10^{-2} A

The distance between the gap of the tetrode and the tip of the coaxial power coupler has to be carefully chosen such that the $e^- e^+$ beams are accelerated with the maximum voltage. In other words, the impedance which represents the beam “seen” by the tetrode has to be real. In the acceleration mode, there is high current (low voltage) at the coupler tip and high voltage (low current) in the tetrode gap. Therefore, the distance between the gap of the tetrode and the coupler tip has to be adequately chosen. In addition, coaxial waveguide transformers are needed to map the low current and high voltage at the tetrode gap into a lower current and higher voltage in the cavity. They must be incorporated into the transmission line at a location of real impedance.

For both reasons in this particular application it is important to know the distances and the corresponding field distribution on the transmission line. We have seen that the lumped-element equivalent circuit model serves us as a guide.

8.2 Coupling RF power out of the cavity

8.2.1 The beam-induced RF power

What is highly welcome in the case of acceleration, the high shunt impedance of an s.c. cavity, can be difficult to master for other applications. An accelerating cavity usually does not only resonate on the fundamental mode for acceleration, but also on higher-order modes (HOMs). There are different families of HOMs, TM and TE like modes, of different rotational symmetry (monopole, dipole, quadrupole, etc.). All these can be excited by RF currents in the cavity, provided that one of the current's Fourier components coincides with the resonant frequency of one of the HOMs and the current vector has a component parallel to the HOM's electric field vector. High fields can be generated in this case which, on the one hand, exercise a force on the beam, leading to beam instabilities and even beam loss while on the other, the beam loses energy into electromagnetic energy of the HOMs, which renders the transfer of RF power to beam power less effective. Or, just as bad, the high fields may cause damage to the cavity by, for instance, a thermal breakdown “quench”, driving the cavity surface n.c. in an uncontrolled way. Obviously, the build-up of HOM fields has to be avoided.

The HOM fields can be calculated by making intuitive use of what we learnt previously. We are interested in the steady state HOM voltage, which is induced by the periodic passage of bunches (repetition time T_b), which constitute the beam. We assume that the bunches are infinitely short and that each of them carries a charge q . In the presence of a HOM cavity voltage V_0 the bunch charge does the work W at the cavity voltage $W = qV_0$. Therefore, by energy conservation, the stored energy $U = (1/2)CV_0^2$ is incremented by the amount $\Delta U = CV_0 \Delta V_0 = \omega_0 CV_0 \Delta V_0 / \omega_0 = V_0 \Delta V_0 / (\omega_0 (R/Q)) = qV_0$, which leads to

$$\Delta V_0 = q\omega_0(R/Q). \quad (49)$$

We know from Eq. (27), that under the assumption $1 - 1/(2Q_L)^2 \approx 1$ in absence of an external drive generator, a voltage V_0 in the cavity decays as

$$V_0(t) = V_0 \exp[-\omega_0 t / (2Q_L)] \exp(j\omega_0 t). \quad (50)$$

Let us assume that immediately after the bunch passage the HOM voltage amplitude in the cavity is $V_0 + \Delta V_0$. Before the passage of the next bunch it will decay and change its phase according to Eq. (50) and, by superposition, equals V_0

$$V_0 = (V_0 + \Delta V_0) \exp[-\omega_0 T_b / (2Q_L)] \exp(j\omega_0 T_b). \quad (51)$$

After a short calculation we get

$$V_0 = \Delta V_0 \exp(j\omega_0 T_b) \exp[-\omega_0 T_b / (2Q_L)] / \{ 1 - \exp(j\omega_0 T_b) \exp[-\omega_0 T_b / (2Q_L)] \}. \quad (52)$$

The “fundamental theorem of beam loading” states that the bunch traversing a cavity is exposed to half of the voltage generated by itself during its passage [34]. Therefore, the average voltage to which the bunch is exposed is $\langle V_0 \rangle = V_0 + \Delta V_0 / 2$ and we obtain

$$\langle V_0 \rangle = (\Delta V_0 / 2)F = (q\omega_0(R/Q)/2)F, \quad (53)$$

with

$$F = \{ 1 + \exp(j\omega_0 T_b) \exp[-\omega_0 T_b / (2Q_L)] \} / \{ 1 - \exp(j\omega_0 T_b) \exp[-\omega_0 T_b / (2Q_L)] \}. \quad (54)$$

With the average beam current $\langle I_b \rangle = q/T_b$, the Fourier component of the RF current at the HOM frequency is $2 \langle I_b \rangle$ under the assumption of infinitely short bunches. The deposited average power P_{HOM} into one HOM of the cavity is

$$P_{HOM} = (1/2) \operatorname{Re}(\langle V_0 \rangle 2 \langle I_b \rangle^*) = (1/2) \omega_0 T_b (R/Q) \langle I_b \rangle^2 \operatorname{Re} F, \quad (55)$$

$$\operatorname{Re} F = \{ 1 - \exp(-\omega_0 T_b / Q_L) \} / \{ 1 - 2 \exp[-(\omega_0 T_b / (2Q_L))] \cos(\omega_0 T_b) + \exp(\omega_0 T_b / Q_L) \},$$

where Re means real part and the asterisk marks the complex conjugate number. If the subsequent bunch does not “see” any voltage amplitude left behind from the previous one, $2Q_L \ll \omega_0 T_b$, $F = 1$,

$$P_{HOM} = (1/2) \langle I_b \rangle^2 T_b \omega_0 (R/Q). \quad (56)$$

On the other hand, in the “worst” case, if the subsequent bunch sees all of the voltage amplitude left behind from the previous one, $\omega_0 T_b \ll 2Q_L$ and, in addition, the bunch repetition time is such that $\exp(j\omega_0 T_b) = 1$, we have $F = 4Q_L / (\omega_0 T_b)$, hence

$$P_{HOM} = 2 \langle I_b \rangle^2 (R/Q) Q_L. \quad (57)$$

P_{HOM} is dissipated partly in R_i , outside the cavity, partly in R , inside the cavity:

$$P_{HOM} = P_{rad} + P_c = P_{rad} (1 + P_c/P_{rad}) = P_{rad} (1 + Q_{ext}/Q_0). \quad (58)$$

Hence

$$P_{\text{rad}} = P_{\text{HOM}} / (1 + Q_{\text{ext}}/Q_0), \quad (59)$$

and

$$P_c = P_{\text{HOM}} - P_{\text{rad}} = P_{\text{HOM}} / (1 + Q_0/Q_{\text{ext}}). \quad (60)$$

Figure 12 shows the power deposited into the TM_{011} mode for LEP, calculated from Eq. (55), with the cavity tuning as parameter. Only if the beam current's Fourier component coincides with the resonant frequency of the HOM ($\cos(\omega_0 T_b) = 1$), the RF power P_{HOM} deposited into the HOM of the cavity increases with the loaded Q value Q_L (up to some limiting Q value $Q_L \rightarrow Q_0$). If not, there exists a Q_L , above which P_{HOM} decreases thanks to non-synchronous movement of the bunch and the RF wave (detuning). P_{HOM} becomes independent of Q_L for low Q_L ($Q_L \leq 10000$), when the bunch-induced field completely decays before the next bunch arrives. The HOM power can attain rather high values and requires dissipation into a room temperature load. We see that by a careful design of the HOM coupler, $Q_{\text{ext}} \ll Q_0$, P_c can be kept tolerably small: $P_{\text{rad}} \approx P_{\text{HOM}}$, $P_c \approx P_{\text{HOM}} Q_{\text{ext}} / Q_0$.

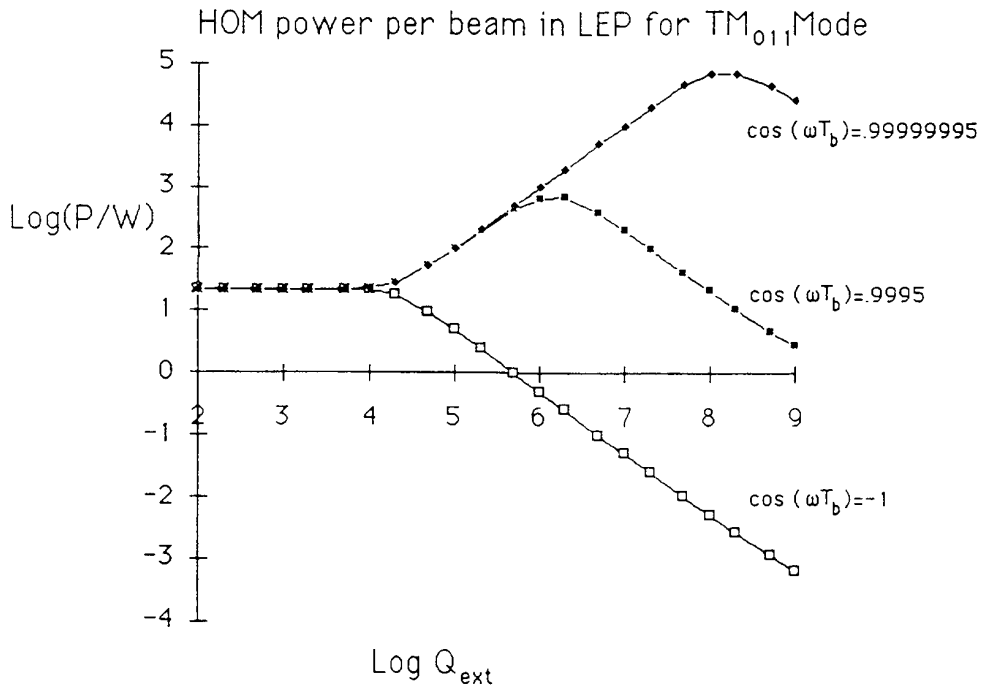


Fig. 12 Power deposited into the TM_{011} mode at 638 MHz for LEP (four bunches, 0.75 mA per bunch, $R/Q = 55 \Omega$) with the mode frequency ω_0 as parameter

8.2.2 Damping the beam induced RF power

Damping of the beam-induced voltage at HOM cavity frequencies is accomplished by specially designed antennas, which do not extract the RF power in the fundamental mode but only in the HOMs. This can be achieved by a coupler as shown, for instance, in Fig. 13 [35], with the corresponding lumped-element equivalent circuit model of Fig. 14. The experimentally determined Q_{ext} are also shown in Fig. 13. A transfer function can be defined as the ratio of the output voltage across the resistor to the input current at the coupler tip [36]. The measured transfer function (Fig. 15) is compared to the computed-one (insert), based on the model of Fig. 14. The cavity field supplies a current to the coupler, which for the fundamental mode frequency is short-circuited by a series resonator (notch filter). The impedance is zero and there

is consequently no current through the load resistor. Hence the fundamental mode is not affected. At higher frequencies, the notch filter becomes an inductance, the total input impedance has a non-vanishing real part and a current flows through the load resistor at room temperature. Note that this coupler geometry allows coupling to both electric and magnetic fields. Only electric field coupling is analyzed here.

Mode	Freq.[MHz]	Q_{ext}
TE 111	462	17000
TE 111	476	14000
TM 110	506	5600
TM 110	515	5700
TM 011	639	10000
TM 111	688	1000
TM 012	1006	<2000

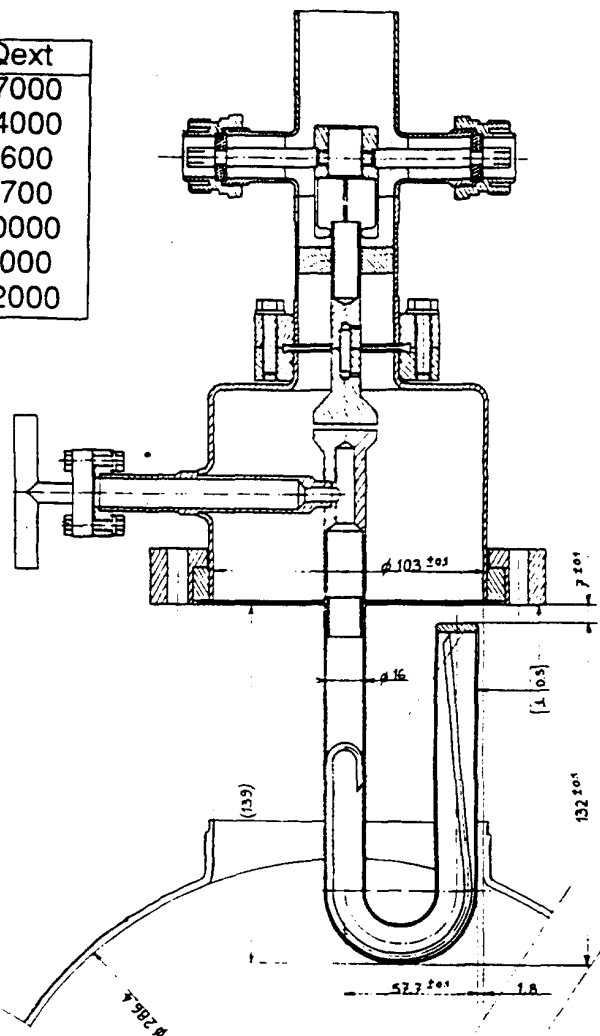


Fig. 13 HOM coupler for LEP type cavities.

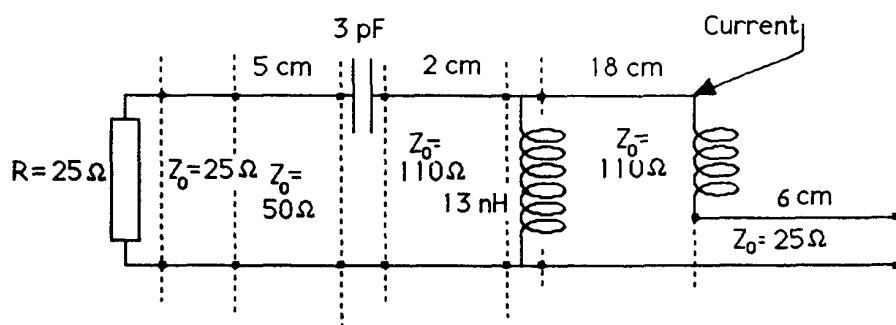


Fig. 14 Lumped-element equivalent circuit model for HOM coupler of Fig. 13

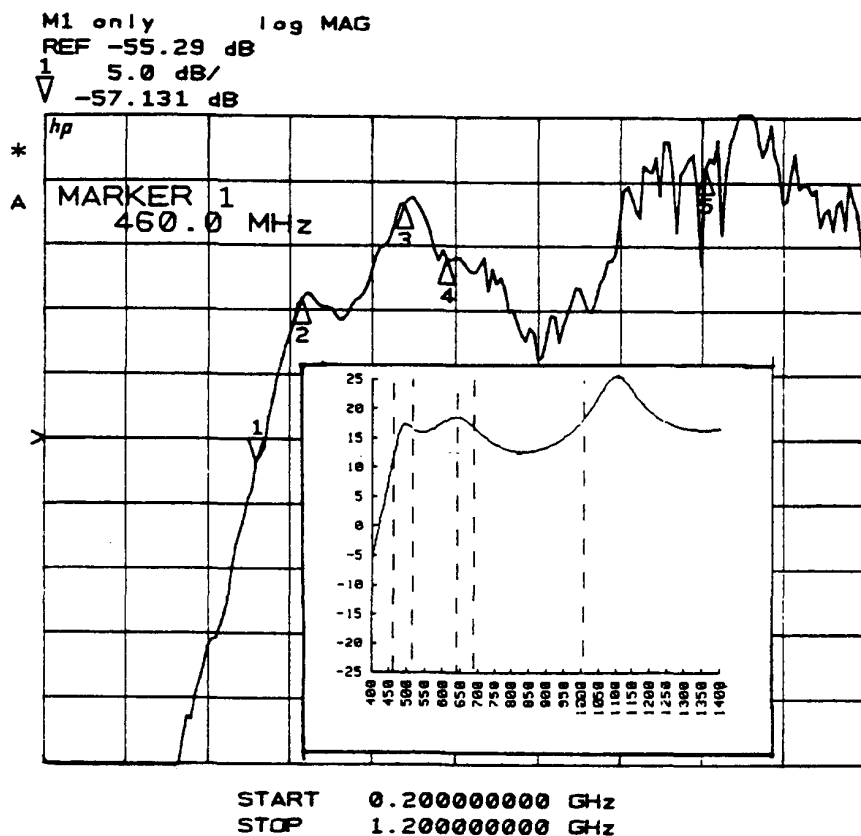


Fig. 15 Transfer function for the HOM coupler of Fig. 13. The insert shows the computed values.

There are applications — we already mentioned in sect. 8.1 the operation of an s.c. cavity in the CERN SPS — for which the fundamental mode has to be damped. An acceleration cycle of e^- and e^+ is interleaved with a cycle of a p beam passage. A most elegant way is to use RF feedback, where the electromagnetic field in the cavity is the replica of a reference signal. During the acceleration cycle, the reference signal corresponds to the accelerating voltage; during the passage of the proton beam, the reference signal is zero. The proton beam-induced voltage is thus cancelled by the injection of RF power into the cavity. As in all feedback systems, oscillations may occur and the limit of stability has to be calculated. It turned out that for this particular layout the minimum cavity impedance was $320 \text{ k}\Omega$, more than a factor 10^6 lower than the undamped cavity [33].

9. TUNING SUPERCONDUCTING CAVITIES

Tuning of an accelerating cavity has two objectives, dynamic tuning during operation and static tuning to obtain a sufficiently “flat” field distribution. “Flat” means that the field amplitude in different cells of a multicell cavity is the same.

The cavity resonance frequency has to be near to a multiple of the revolution frequency of the beam. This is generally accomplished by a frequency tuner, which adjusts the resonance frequency to a stable master generator frequency. The frequency tuner makes use of the fact that, according to Slater’s theorem, a deformation of the cavity shape may change the stored electric energy in a different way than the stored magnetic energy. To make them equal again the resonance frequency will change. Of course, all external forces may also alter the cavity shape and so the resonance frequency, which has to be readjusted by the tuner. Particularly

cumbersome can be mechanical oscillations of the cavity driven by pressure oscillations of the helium. Therefore, the tuner feedback circuit has to react fast enough without causing oscillations.

The accelerating cavities used nowadays are tuned by a mechanical change of the total length, either accomplished by an electric motor or, to avoid jamming at low temperatures, by piezo-electric action [37], thermal or/and magnetostrictive action on a supporting bar of ferromagnetic material like nickel [38].

For economical reasons the accelerating cavity usually consists of several monocells electromagnetically coupled together with one feed for RF power. If the field excitation in the different monocells were quite different, for a fixed total accelerating voltage there is one monocell with high field excitation. As the losses and the probability for defects causing a quench increase non-linearly with field, the performance of the cavity is inferior to that of a cavity with flat field distribution. Therefore, the cavity needs to be statically tuned to achieve field flatness, mostly achieved by inelastic deformation of the relevant monocells. We will outline the tuning procedure by taking as an example a three-cell cavity, modelled in Fig. 16 very similarly to Ref. [39]. By applying Kirchhoff's voltage rules to each cell we get, after differentiating, the following set of equations.

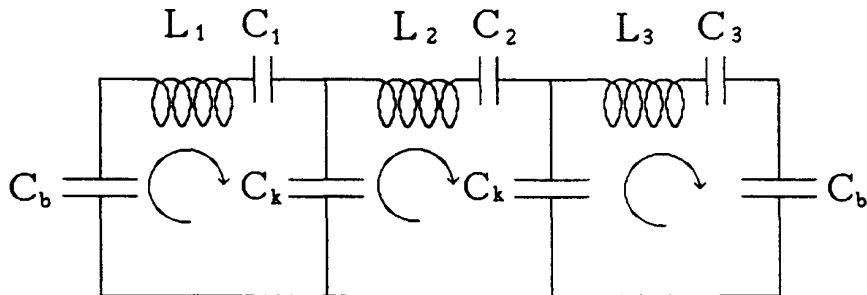


Fig. 16 Lumped-element equivalent circuit model for a three-cell cavity

$$(1/C_b)I_1 + L_1(d^2/dt^2)I_1 + (1/C_1)I_1 + (1/C_k)(I_1 - I_2) = 0 , \quad (61)$$

$$(1/C_k)(I_2 - I_1) + L_2(d^2/dt^2)I_2 + (1/C_2)I_2 + (1/C_k)(I_2 - I_3) = 0 ,$$

$$(1/C_k)(I_3 - I_2) + L_3(d^2/dt^2)I_3 + (1/C_3)I_3 + (1/C_b)I_3 = 0 .$$

With the shorthand

$$1/C_b + 1/C_1 + 1/C_k = 1/C'_1 , \quad (62)$$

$$1/C_2 + 2/C_k = 1/C'_2 ,$$

$$1/C_b + 1/C_3 + 1/C_k = 1/C'_3 ,$$

we have

$$[L_1(d^2/dt^2) + (1/C'_1)]I_1 - (1/C_k)I_2 = 0 , \quad (63)$$

$$-(1/C_k)I_1 + [L_2(d^2/dt^2) + (1/C'_2)]I_2 - (1/C_k)I_3 = 0 ,$$

$$-(1/C_k)I_2 + [L_3(d^2/dt^2) + (1/C'_3)]I_3 = 0 .$$

With

$$\omega_1^2 = 1/(L_1C'_1), \omega_2^2 = 1/(L_2C'_2), \omega_3^2 = 1/(L_3C'_3) , \quad (64)$$

$$C'_1/C_k = k_1, C'_2/C_k = k_2, C'_3/C_k = k_3 , \quad (65)$$

$$\vec{I} = (I_1, I_2, I_3)^T , \quad (66)$$

$$(d^2/dt^2) \vec{T} = -\Omega^2 \vec{T}, \quad (67)$$

we have to solve the eigenvalue problem

$$\begin{pmatrix} \omega_1^2 & -k_1\omega_1^2 & 0 \\ -k_2\omega_2^2 & \omega_2^2 & -k_2\omega_2^2 \\ 0 & -k_3\omega_3^2 & \omega_3 \end{pmatrix} \vec{T} = \Omega^2 \vec{T}. \quad (68)$$

For $k_1 = k_2 = k_3$, $\omega_1 = \omega_2 = \omega_3 = \omega$, we get

$$\begin{pmatrix} \omega & -k\omega & 0 \\ -k\omega & \omega & -k\omega \\ 0 & -k\omega & \omega \end{pmatrix} \vec{T} = \Omega^2 \vec{T}. \quad (69)$$

with the eigenvalues for the $\pi/3$, $2\pi/3$ and π mode,

$$\begin{aligned} \Omega_1^2 &= \Omega_{\pi/3}^2 = \omega^2(1 - \sqrt{2}k), \quad \Omega_2^2 = \Omega_{2\pi/3}^2 = \omega^2, \\ \Omega_3^2 &= \Omega_\pi^2 = \omega^2(1 + \sqrt{2}k), \end{aligned} \quad (70)$$

and eigenvectors

$$\begin{aligned} \vec{T}_{\pi/3} &= (1/2, (1/2)\sqrt{2}, 1/2)^T, \quad \vec{T}_{2\pi/3} = (1/\sqrt{2}, 0, -1/\sqrt{2})^T, \\ \vec{T}_\pi &= (1/2, -(1/2)\sqrt{2}, 1/2)^T, \end{aligned} \quad (71)$$

respectively.

The coupling constant k is related to the frequency difference $\Delta\Omega$ of the π and $2\pi/3$ mode

$$k = (1/\sqrt{2}) \Delta\Omega/\omega. \quad (72)$$

We see that for equal cell frequencies ω the cell excitation is non-uniform. If we want to have uniform cell excitation, we can solve Eq. (68) with $\vec{T} = (1, -1, 1)^T$, and $k = k_1 = k_2 = k_3$, $\omega_3 = \omega_1$,

$$\begin{pmatrix} \omega_1^2 & -k\omega_1^2 & 0 \\ -k\omega_2^2 & \omega_2^2 & -k\omega_2^2 \\ 0 & -k\omega_1^2 & \omega_1^2 \end{pmatrix} \begin{pmatrix} 1 \\ -1 \\ 1 \end{pmatrix} = \Omega_\pi^2 \begin{pmatrix} 1 \\ -1 \\ 1 \end{pmatrix}. \quad (73)$$

The result is

$$\omega_1^2 = \Omega_\pi^2/(1 + k), \quad \omega_2^2 = \Omega_\pi^2/(1 + 2k), \quad \omega_3^2 = \Omega_\pi^2/(1 + k). \quad (74)$$

The tuning of a multicell cavity is an iterative procedure. With k from Eq. (72) and from the experimentally determined field flatness in the π mode $\vec{T}_\pi = (I_1, I_2, I_3)^T$ the individual cell frequencies ω_i ($i = 1, 2, 3$) are given by:

$$\begin{aligned} \omega_1^2 &= [I_1/(I_1 - k I_2)] \Omega_\pi^2, \\ \omega_2^2 &= \{ I_2/[I_2 - k(I_1 + I_3)] \} \Omega_\pi^2, \\ \omega_3^2 &= [I_3/(I_3 - k I_2)] \Omega_\pi^2. \end{aligned} \quad (75)$$

From the comparison with Eq. (74) the necessary frequency shift to be applied to each individual cell can be derived. This can be achieved by inelastic deformation of the cell length by an amount which has to be determined experimentally.

10. DESIGN CRITERIA AND THE STATE OF THE ART

Development of s.c. accelerating cavities started about three decades ago. Within this time their design at the different laboratories has converged a lot (Fig. 17). Generally accepted is the "spherical" shape with slightly inclined iris, combining several advantages:

- electron multipacting is largely suppressed,
- good compatibility with sheet-metal fabrication techniques,
- relatively high mechanical stability,
- easy draining of polishing and cleaning liquids.

The sheet-metal construction technique has prevailed. The thin wall allows better cooling and better access of the liquid helium to the iris. It is a relatively cheap technique, and it allows joining of parts by electron beam (EB) welding, or even shaping of whole parts by hydraulic forming. The larger fabrication tolerances can be corrected relatively easily by inelastic deformation of the cells. It allows frequency tuning by changing the overall length in a controlled way.

One has to admit, however, that mechanical vibrations, which may plague their operation considerably, are favoured by this construction technique. If these vibrations cannot be sufficiently damped by stiffeners, an effort should be made to shift them to higher frequencies. One can then hope that it is less likely for them to be excited.

Couplers for power input and HOM suppression are mostly of a compact coaxial layout, absolutely necessary at frequencies below, say, 1 GHz. Windows should be located, if possible, between the beam and insulation tank vacuum, to reduce the consequences if they crack.

Frequency tuners without moving parts are advantageous, because they avoid jamming at low temperatures.

All holes in the cavity cells themselves are dangerous, because they increase the probability for multipacting. Therefore, HOM and power coupler parts are attached to the beam tube; plunger tuners are not used.

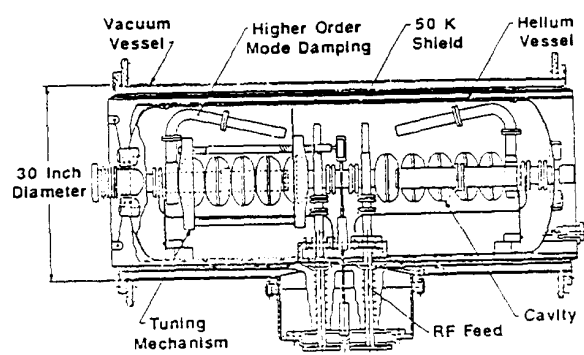
The number of cells is limited so that the HOMs can be sufficiently damped by the beam tubes, and the RF power to be transferred can be tolerated. Both constraints depend very much on the features of the accelerator (voltage, current, bunch length, etc.).

By means of the reliable computer codes generally adopted nowadays the shape of the cavity has to be "fine-tuned" for several, sometimes contradicting, constraints.

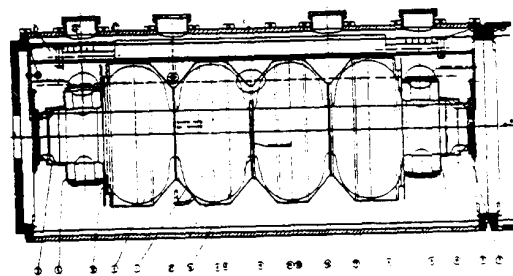
The cryostat can be designed to give access to vital parts (tuners, couplers, temperature probes, etc.), without the need to break the cavity vacuum or to remove the cryostat from the beam line.

Table 9 shows electron accelerators based completely or in part on the s.c. RF technology. The pioneering one at HEPL of Stanford University and the s.c. microtron at the University of Illinois (Urbana) were not free from electron multipacting. What I call the "total RF voltage installed" is based on the design value for the accelerating gradient and the actual number of s.c. RF cavities in the accelerator. Under operating conditions, the total voltage obtained is somewhat lower than the installed one. The maximum gradient is understood to be achieved with an individual cavity connected with the beam vacuum.

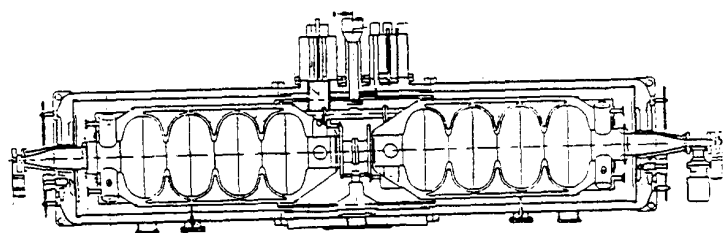
The gradient obtained under operating conditions is lower than the design gradient of 5 MV/m in almost all examples. But progress is fast, and it is difficult to keep trace of the latest numbers from the various laboratories. It is generally accepted that a gradient of 5 MV/m can be mastered in large modules. To obtain higher gradients, the field emission loading has to be better controlled by improved surface processing. The potential for higher fields exists. Let us grasp it!



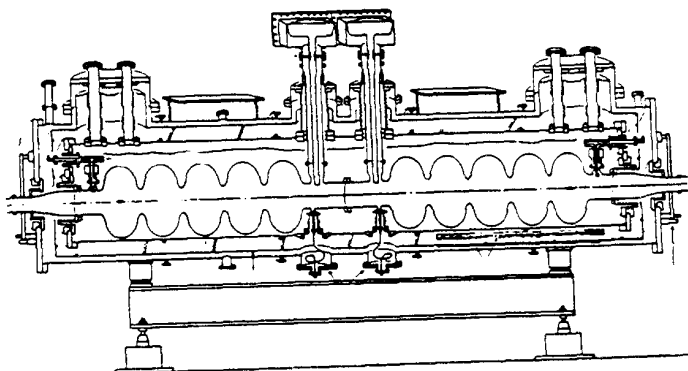
CEBAF



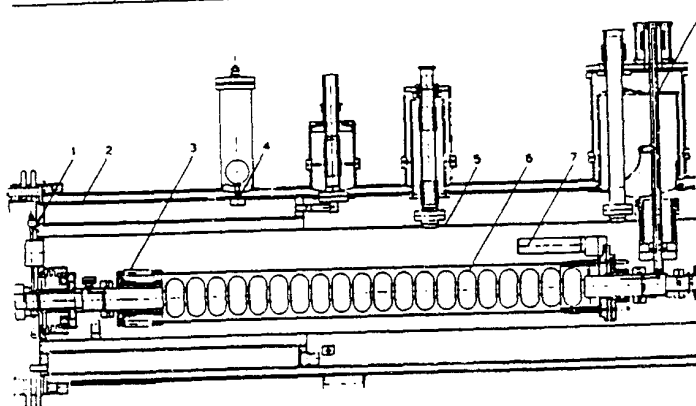
CERN



DESY



KEK



Wuppertal/Darmstadt

Fig. 17 Cavity shapes

Table 9
RF s.c.-based electron accelerators or accelerators with s.c. cavities permanently installed

Laboratory	Year	Freq. [GHz]	Total installed voltage [MV] ^(a)	Total obtained voltage [MV]	Max. gradient obtained [MV/m]	Refs
HEPL	1977	1.3		50	2.2 ^(b)	[40]
U Illinois (MUSL-2)	1977	1.3		13	2.3 ^(b)	[41]
CERN (SPS)	1988–1991	0.35	8.5	12	7.1	[42]
U Darmstadt (SDALINAC)	1989–1991	3.0	50	~ 43	6.7	[43]
KEK (TRISTAN)	1989–1991	0.5	240	220	8.6	[44]
CERN (LEP)	1990–1991	0.35	68	54	5.0	
DESY (HERA)	1991	0.5	48	32	5.0	[45]
CEBAF	1991	1.5	25	28	8.0	[46]

(a) Design gradient 5 MV/m.
(b) Structure design not multipactor free.

Acknowledgements

I would like to thank my colleagues from CERN for many ideas and fruitful discussions.

REFERENCES

- [1] H. Piel, proc. CERN Acc. School, Hamburg (1988), ed. S. Turner, Yellow Report CERN 89-04 (1989) 149.
H. Lengeler, *Ibid.*, 197.
- [2] W. Weingarten, Particle World 1/4 (1990) 93.
- [3] P. Lebrun, *Ibid.* ref. [1] 41.
- [4] A.B. Pippard, Rep. Prog. Phys. 23 (1960) 176.
- [5] W. Meissner and R. Ochsenfeld, Naturwissenschaften 21 (1933) 787.
- [6] F. London and H. London, Zeitschr. für Phys. 96 (1935) 359;
F. London, Une conception nouvelle de la supraconductivité, Paris (1937).
- [7] J.D. Mattis and J. Bardeen, Phys. Rev. 111 (1958) 412;
A.A. Abrikosov, L.P. Gor'kov and I.M. Khalatnikov, Sov. Phys. JETP 8 (1959) 182.
- [8] J.P. Turneaure, Thesis, W.W. Hansen Lab. Stanford Univ., Stanford, CA, USA (1967).
- [9] T. Yogi, G.J. Dick and J.E. Mercereau, Phys. Rev. Lett. 39 (1977) 826.
- [10] Y. Bruynseraede et al., Physica 54 (1971) 137.
- [11] D. Schnitzke et al., Phys. Lett. A45 (1973) 241.
- [12] H. Padamsee et al., IEEE Trans. Mag. MAG-15 (1979) 602.
- [13] B. Hillenbrand et al., IEEE Trans. Mag. MAG-13 (1977) 491.
- [14] B. Pioszyk et al., Trans. Nucl. Sci. NS-20 (1973) 108.
- [15] C. Benvenuti et al., proc. IEEE Part. Acc. Conf. San Francisco (1991), to be published.
- [16] U. Klein, Thesis, Wuppertal Univ., WUB-DI 81-2 (1981).
- [17] J.P. Turneaure, IEEE Nucl. Sci. NS-18 (1971) 166.
- [18] J.P. Turneaure, Appl. Supercond. Conf., Annapolis, MD, USA (1972) 621.
- [19] H. Lengeler et al., IEEE Trans. Mag. MAG-21 (1985) 1014.
- [20] P. Kneisel et al., Appl. Supercond. Conf., Annapolis, MD, USA (1972) 657.
- [21] J.P. Turneaure and Nguyen Tuong Viet, Appl. Phys. Lett. 16 (1970) 333.
- [22] M.A. Allen et al., IEEE Trans. Nucl. Sci. NS-18 (1971) 168.
- [23] A. Philipp, Thesis, Kernforschungszentrum Karlsruhe, KfK-3268 (1982).
- [24] G. Müller, Thesis, Wuppertal Univ. WUB-DI 83-1 (1983).
- [25] H. Padamsee et al., IEEE Trans. Mag. MAG-19 (1983) 1308.
- [26] H. Padamsee, proc. 2nd Workshop on RF Superconductivity, ed. H. Lengeler, CERN, Geneva (1984) 339.

REFERENCES (cont'd)

- [27] U. Klein and D. Proch, proc. Conf. on Future Possibilities for Electron Accelerators N1–N17, eds J.S. MacCarthy and R.R. Whitney, Charlottesville, VA, USA (1979).
V. Lagomarsino et al., IEEE Trans MAG–15 (1979) 25.
- [28] W. Weingarten, IEEE Trans. Electr. Insul. 24 (1989) 1005.
- [29] Koichi Yabe et al., 9th ICCCS proc. Institute of Environmental Sciences (1988) 509.
- [30] D. Proch, proc. EPAC, Rome, ed. S. Tazzari (1988) 29.
- [31] E. Haebel (private communication).
- [32] G. Cavallari et al., proc. 3rd Workshop RF Superconductivity, ed. K.W. Shepard, Argonne, Ill. USA (1987) ANL-PHY-88-1, 565.
- [33] D. Boussard et al., Ibid. ref. [30] 985;
P. Bernard et al., Ibid. ref. [30] 988.
- [34] P. Wilson, Physics of High-Energy Particle Accelerators, Fermilab Summer School (1981); and American Institute of Physics, New York (1982) 452.
- [35] E. Haebel et al., in preparation.
- [36] E. Haebel, Ibid. ref. [26] 299.
- [37] V. Aab et al., proc. 3rd Workshop RF Superconductivity, ed. K.W. Shepard, Argonne, Ill. USA (1987) ANL-PHY-88-1, 127.
- [38] G. Cavallari et al., Ibid. ref. [31] 625.
- [39] E. Haebel and J. Tückmantel, CERN/EF/RF 81–05 (1981).
- [40] J.R. Calarco et al., IEEE Trans. Nucl. Sci. NS–24 (1977) 1091.
- [41] P. Axel et al., Ibid. ref. [40] 1133.
- [42] D. Boussard et al., proc. IEEE Part. Acc. Conf. Chicago (1989) 1783.
- [43] H.D. Gräf, private communication.
- [44] K. Akai et al., Ibid. ref. [15] to be published.
- [45] D. Proch, Ibid. ref. [15] to be published.
- [46] K. Jordan et al., Ibid. ref. [15] to be published.